Dissociative attachment of low-energy electrons to state-selected diatomic molecules

M. Külz, M. Keil, A. Kortyna,* B. Schellhaaß, J. Hauck, and K. Bergmann
Fachbereich Physik der Universität Kaiserslautern, Postfach 3049, D-67653 Kaiserslautern, Germany

W. Meyer and D. Weyh
Fachbereich Chemie der Universität Kaiserslautern, Postfach 3049, D-67653 Kaiserslautern, Germany

(Received 25 July 1995; revised manuscript received 26 January 1996)

The dissociative attachment process in low-energy collisions [$Na_2(v'',j'')+e^- \rightarrow Na + Na^-$, with electron energies <1.0 eV] is studied as a function of vibrational excitation over a broad range of excited levels. We employ a crossed electron-molecule beams arrangement and two optical methods for preparing vibrationally excited states: Franck-Condon pumping (FCP) as well as the efficient and highly state-specific technique of stimulated Raman scattering with adiabatic passage (STIRAP). Both methods are capable of preparing vibrational levels with energies up to about 60% of the $Na_2 X^1\Sigma_g^+$ binding energy ($v'' \leqslant 30$). Analysis of the FCP data shows an increase of more than three orders of magnitude in the state-dependent dissociative attachment rate as a function of the vibrational level up to $v''=12$. For $v''>12$, which is close to the exoergic threshold, no further increase with v'' is observed. The dissociative attachment rates measured for single rovibronic states using the STIRAP technique confirm the validity of the conclusions drawn from our analysis of the FCP measurements. The potential curve of the $Na_2^- A^2\Sigma_g^+$ state, which is essential for the dissociative attachment process, has been determined from variational valence shell multireference configuration interaction calculations in its bound region but by imposing Feshbach projection in its resonance region. The crossing of this potential with that of the $Na_2(X)$ state is found between $v''=11$ and $v''=12$, in full agreement with the conclusions from analysis of the experimental data. The variation of the theoretical enhancement factors with the electron energy, calculated in the framework of the traditional resonance theory, are also reported. After convolution with the electron flux distribution, good agreement with the experimental enhancement factors is found.

PACS number(s): 34.80.Ht, 31.25.Nj, 34.80.Qb

I. INTRODUCTION

The vibrational level dependence of the dissociative attachment (DA) of electrons to diatomic molecules, e.g., $Na_{2(v'')+e} \rightarrow Na+Na^-$, results from the coupling of the nuclear degrees of freedom with the motion of the outermost electrons. The high sensitivity of the DA cross section to vibrational excitation [1–9] enables a delicate experimental test of theoretical predictions. In particular, DA measurements may reveal details of the coupling between negative ionic resonance states and the continuum in which they are embedded. It is also expected that nonlocal contributions to the molecular potentials will ultimately be found to be important in describing the dynamics of the DA process for slow electrons [10].

Interest in the effect of vibrational excitation on the DA cross section was initiated by the discovery of an anomalously large O^- signal created by low-energy electron bombardment of atomic oxygen [11]. The O^- signal was traced to the DA of O_2 that had been vibrationally excited by the mechanisms used to create atomic oxygen (either a gas discharge or thermal dissociation). In further studies, thermally excited low-lying vibrational levels of O_2 were used and it was concluded that the DA cross section for vibrationally excited states is much larger than had previously been expected [12,13]. In the case of H_2, the theoretically [2–5,14] and experimentally [1] well-known effect of DA and its cross section is even used to determine the rovibronic population of the molecule by observing the variation of the H^- production rate with the energy of the incident electrons [15].

Today, DA is a well-studied phenomenon, albeit most investigations have not attempted to control internal state distributions. Absolute DA cross sections have been measured for a wide variety of molecules [16], including Na_2 using an effusive beam apparatus [17]. Even though no state selectivity was provided in the latter work, the authors conclude from their measured energy dependence of the DA cross section that the observed DA signal was dominated by thermally populated vibrationally excited states, which implies that the DA cross sections increase sharply with internal excitation.

A. The resonance model

The resonance model of the DA process [14,18,19] assumes that the interaction between a neutral molecule and a unbound electron may lead to the formation of a temporary negative ion state. Figure 1 illustrates the relevant potential energy curves for Na_2+e^-. If the Born-Oppenheimer approximation applies to this situation, an electron can attach to a neutral molecule only if the collisional kinetic energy is equivalent to the difference between the potential energies in the molecular neutral and ionic states. The internuclear sepa-

*Present address: Jet Propulsion Laboratory, M/S 121-104, California Institute of Technology, 4800 Oak Grove Drive, Pasadena, CA 91109-8099.

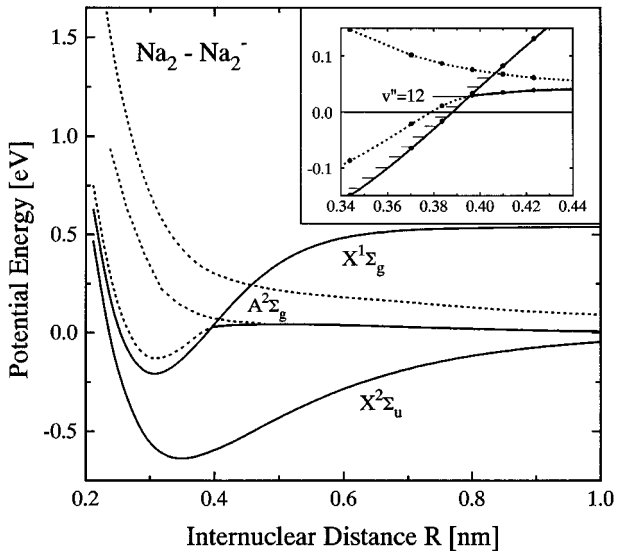

FIG. 1. Molecular potential curves relevant to the dissociative attachment process in Na_2. Solid lines: bound states from variational MR-CI calculations for valence shell electrons. Lower dashed line: $Na_2(X)+e^-(\sigma_g)$ from variational MR-CI for the finite basis specified in the text. Upper dashed line: pure core-excited component of the $Na_2^-(A)$ state. Middle dashed line: suggested Na_2^- $A^2\Sigma_g$ resonance state as obtained from MR-CI with Feshbach projection (see text). Inset: enlarged crossing region with $Na_{2(X)}$ vibrational energy levels.

ration where the attachment takes place is usually referred to as the capture radius R_c. However, the newly formed ion is unstable and may undergo autodetachment with a lifetime $1/\Gamma$, where Γ is the energy width of the ionic state, perhaps leaving the molecule with vibrational excitation. Alternatively, the ion may stabilize through dissociation: when the internuclear distance increases beyond the crossing of the *resonance* ionic state with the ground state (see Fig. 1), and if the ionic potential does not exhibit a barrier at larger R, the system will dissociate into a neutral atom and a negative ion. This crossing point, beyond which ejection of the resonantly attached electron becomes energetically forbidden in the Born-Oppenheimer approximation, is known as the stabilization radius R_s. If the resonance state is short lived and R_s is significantly larger than the outer turning point of low-lying vibrational states, as in the case of $H_2^-(^2\Sigma_u^+)$, one may find an increase in the DA cross section of many orders of magnitude as a function of vibrational excitation until the neutal molecules outer turning point exceeds R_s. Above the exoergic limit the DA cross section has been found to remain more or less constant or to decrease slightly.

In summary, DA occurs when an incident electron is captured into a resonance state that subsequently survives long enough for the internuclear separation to exceed the stabilization radius R_s. The probability for the competing autodetachment channel is generally assumed to be proportional to the exponential function of the integrated width of the resonance state, i.e., $\exp[\int_{R_c}^{R_s}\Gamma(R')(dR'/dt)^{-1}dR']$. Since $\Gamma(R')$ tends to decrease with increasing $R'<R_s$, one may expect a strong increase of DA for vibrational levels below the exoergic limit, which may total to an increase with v'' over several orders of magnitude.

B. The electronic states involved

The vibrational enhancement of DA has also been intensively studied theoretically; useful reviews may be found in Refs. [10] and [20]. The most rigorous treatments, including the determination of electronic resonance state properties as well as local and nonlocal dynamics calculations, have been applied to the DA process for H_2+e^- [1–5]. For the two lowest resonances related to the electronic structures $^2\Sigma_u^+(1\sigma_g^2 1\sigma_u)$ and $^2\Sigma_g^+(1\sigma_g 1\sigma_u^2)$, quite different results were obtained: For the short-lived but attractive $^2\Sigma_u^+$ shape resonance, a nearly vertical onset with electron energy and dramatic enhancement with increasing v'' was found. For the relatively long-lived but purely repulsive $^2\Sigma_g^+$ resonance, which is of mixed Feshbach and shape structure, a much smoother onset and a relatively small vibrational enhancement was obtained. The results of several calculations are available for low-lying ionic states of the alkali dimer Li_2 [21–23]. The attachment process was treated using the local approximation [3]. To the best of our knowledge, reliable theoretical data for Na_2^- are restricted to the ground-state potential and radii greater than the stabilization radius for the lowest resonance state [22,24]. In contrast to the electronically similar H_2, the lowest negative ion state of alkali dimers is purely bound and does not contribute to the DA process. The lowest alkali resonance has $^2\Sigma_g^+$ symmetry and is again of mixed Feshbach and shape structure but it is considerably attractive in Li_2^- and, according to Ref. [22], apparently rather flat for Na_2^- down to the equilibrium internuclear distance of $Na_{2(X)}$. The resonance parts of the potential curves have in all cases been obtained by restricting the one-electron space to compact L^2 functions, which have either been optimized in the asymptotic region [21,23] or have been extrapolated smoothly from optimizations in the region where the state is still bound [22]. Not surprisingly, the minimum of this resonance state of Li_2^- varies between 1300 and 2200 cm^{-1} and it is not clear how well the most elaborated potential with a minimum of 1470 cm^{-1} [23] represents the true position of the resonance. This is most precarious because the energetic position of the resonance also serves to derive the width of the state by Wigner's threshold law for s electrons. Using this input in a local treatment of the DA dynamics, Wadehra [3] derived a factor of 15 enhancements in the Li_2 DA cross section for $v''=2$ (as compared to the cross section for $v''=0$) and a maximum enhancement of 50 for $v''=7$ and 8, which bracket the Li_2-Li_2^- crossing point. This is compatible with the rather inconclusive measurements on Li_2[25] but it is in contrast to the large enhancements found here for Na_2, namely, ~ 500 for $v''=10$ and ~ 2000 for $v''=12$.

C. Previous experimental DA studies involving vibrationally excited molecules

Theoretical predictions for the vibrational dependence of the DA cross section have been experimentally confirmed for the lowest five vibrational states of H_2 and D_2 [1] and up to $v''=8$ in Ref. [15]. The authors of the former study controlled vibrational excitation through resistive heating of a

target cell containing either H_2 or D_2. In the latter work very high vibrational excitation resulted from the process of surface recombination of H atoms in a microwave discharge. Both of these approaches rely on the relatively large energy gap between the vibrational levels in H_2 and D_2 and an electron beam with a very narrow energy distribution, which thus permitted the DA signal to be resolved into individual vibrational manifolds. Reference [1] reports an increase of several orders of magnitude in the DA cross section for the lowest resonance state. Data from vibrational levels near the exoergic limit, where the vibrational dependence of the DA cross section is expected to change sharply, were not sampled. The lack of data for the DA process involving states above the lowest few vibrational levels is shared by all but a few of the DA studies published to date.

Despite the aforementioned shortcoming, thermal excitation has been used successfully in a number of other studies to measure the effect of low internal excitation on the DA process in various small molecules, e.g., H_2 [26], I_2 [27,28], HCl and HF [29], CO_2 [13], and N_2O [30]. The DA temperature dependence has also been studied in a variety of complex molecules, including SF_6 [31–35], SF_5Cl [35], SO_2F_2 [36], several hydrocarbons [33,37,38], and a number of halogenated compounds [39–42]. Of all of the above cited studies, only Refs. [1,29] provide vibrationally resolved data.

Several other techniques have also been used to prepare vibrationally excited molecules for DA studies. The recombination of hydrogen atoms on surfaces has been used to create vibrationally excited H_2 [43] as has electron impact excitation [44]; however, these two techniques suffer from the disadvantage of preparing ill-defined vibrational distributions. In yet another approach for preparing vibrationally excited molecules, a CO_2 laser has been employed to populate the ν_3 vibrational mode of SF_6 via a direct infrared transition [45].

The above cited studies show that, in general, vibrational excitation leads to an enhancement in the DA rate. The degree of enhancement depends on the exact electronic structure of the molecule under study, but many simple diatomic molecules exhibit large increases in the DA rate even for small increases in vibrational excitation.

Several optical pumping techniques promise to alleviate restrictions inherent in the previously mentioned techniques for preparing vibrationally excited molecules. Franck-Condon pumping (FCP) provides a means for producing and controlling vibrationally excited population distributions. This is done by transferring population from the level $v''=0$ to the electronically excited state, which then decays via spontaneous emission to target vibrationally excited states. In the first application of FCP to study the DA, a fixed frequency laser (the second-harmonic of a Nd:YAG laser) pumped a single $B \leftarrow X$ transition in I_2 [46]. Later, McGeoch and Schlier [25] applied FCP to the study of DA in Li_2 using a tunable pulsed laser system to create several vibrationally excited distributions. They observed little variation of DA rate above the exoergic limit; but a relatively large Li^- background obscured observation of the DA signal from Li_2 in low vibrational levels preventing both the observation of any significant increase in the DA rate as a function of vibrational excitation and the direct comparision of the DA rate at high vibrational levels to that at low vibrational levels.

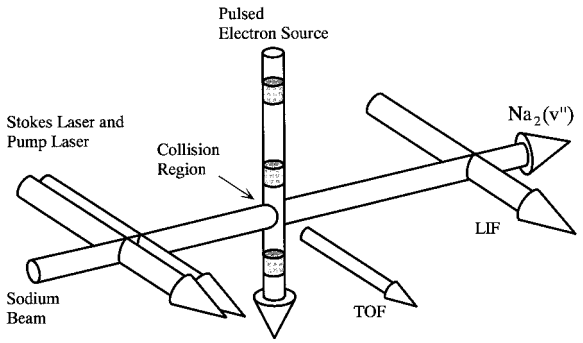

FIG. 2. Schematic diagram of the experimental apparatus.

The current paper is a followup to an earlier work [47] examining the vibrational dependence of the DA rate of Na_2 using FCP. That publication reported an increase in the DA rate (see Fig. 5) of three orders of magnitude. Above the exoergic limit, the DA rate was remarkably insensitive to further increases in vibrational excitation. Here, we expand upon these DA rate measurements by using the highly efficient and selective adiabatic population transfer technique, termed *stimulated Raman scattering with adiabatic passage* (STIRAP). Our objective is (i) to identify the crossing point between the Na_2^- negative ion potential and neutral $Na_2(X)$ potential energy curves and to compare this crossing point to the results from quantum chemical calculations, and (ii) to determine unambigiuously the vibrational dependence of the DA rate at vibrational excitations exceeding the energy at the crossing.

II. EXPERIMENTAL APPARATUS AND METHODOLOGY

A. Particle beams and detection

Our experiment employs a crossed electron-molecule beams arrangement with time-of-flight (TOF) analysis of the resulting negative ions, and laser-based facilities for preparing and probing the excited molecular states (see Fig. 2). The vacuum system includes three differentially pumped chambers ($10^{-5}-10^{-7}$-mbar background pressure). The molecular-beam-source chamber contains a supersonic alkali vapor beam source. Vibrational excitation of the molecules is achieved in the optical-pumping chamber. The scattering chamber contains an electron beam source, a TOF mass spectrometer, and laser-induced fluorescence probing equipment. The laser pumping techniques and the laser probing arrangements are described in more detail below.

The molecular-beam source is of a standard, double-chamber design. The reservoir is typically operated at 900 K and the nozzle is held 50 K hotter. The 50-mbar vapor pressure of sodium at 900 K combined with a 0.4-mm-diam nozzle results in a supersonic expansion producing a molecular beam with a 0.10–0.15 mole fraction of Na_2 [48]. We employ several spectroscopic techniques to characterize the molecular beam. A Doppler-shift technique [49] yields a molecular-beam speed ratio of 5.2, and laser-induced fluorescence measurements demonstrate that the supersonic expansion produces a molecular beam with about 99% of its Na_2 residing in the ground vibrational state. Furthermore, laser-induced fluorescence probing of the ground vibrational state yields a distribution of rotational levels j'' that corre-

sponds to a temperature of 27 ± 1 K for $j''\leqslant14$ and 43 ± 4 K for $j''>14$.

Two heated skimmers restrict the molecular beam to a divergence of 0.7°. The first skimmer is located between the molecular-beam-source chamber and the optical-pumping chamber, while the second skimmer is positioned between the optical-pumping chamber and the scattering chamber. The divergence of the molecular beam was carefully measured to estimate the maximum Doppler shift that would be encountered by a laser beam intersecting the molecular beam at right angles. Keeping this Doppler shift to a minimum is essential for achieving a uniform optical-pumping rate across the beam's azimuthal dimension since the transverse velocity associated with the beam divergence will tend to shift the molecular transition frequency out of resonance with the laser radiation. In fact, a divergence on the order of only a few degrees would decrease the overall optical-pumping efficiency significantly.

After passing through both skimmers the molecular beam enters the scattering chamber and intersects a pulsed, magnetically guided electron beam. Our electron beam source is a pulsed version of the one described in Ref. [50]. Electrons are thermionically emitted from a low-temperature barium oxide cathode. A set of three mesh-covered apertures accelerate the electron beam toward the scattering region. The 0.7-eV full width at half maximum electron energy spread is primarily due to the thermal distribution of the emitted electrons. The magnitude of the magnetic guiding field is approximately 100 G. Negative ions formed in the molecular-beam–electron-beam interaction are mass analyzed by a Wiley and McLaren type TOF mass spectrometer [51]. Ions are collected with a pulsed, 100-V/cm extraction field, pass into a region where they are further accelerated by a second electric field to a total energy of 900 V, and finally enter the TOF field-free region for mass analysis. Ions are detected by a trio of microchannel plates arranged sequentially in a chevron configuration. A 100-G magnetic field can also be applied to the TOF's field-free region to deflect stray electrons (originating from the electron beam) away from the charged particle detector, thereby reducing detector noise and increasing the detector life. This mass spectrometer provides a high repetition rate, good rejection of stray electrons, and a resolution of better than 1 at 23 atomic mass units.

The electron beam and TOF were tested by measuring the energy dependence of O^- production through dissociative attachment of electrons to CO_2 and by observing SF_6^- production from electron attachment to SF_6. These tests accurately reproduced previously reported results [16,35,52]. Because the energy-dependent electron attachment cross section of SF_6 decreases rapidly for collision energies $E>0$, both the electron energy distribution and the zero-energy calibration of our electron beam source can be established by examining the SF_6^- production as a function of electron energy. Figure 3 shows the SF_6^- rate as a function of the electron energy, which is given by the potential difference between the cathode and the collision region. This is a direct measure of the energy distribution of the electron flux.

DA data for both excited- and ground-state Na_2 molecules are collected using the following timing sequence. The electron beam is pulsed for 0.25μs. After a $<0.1\mu$s delay to allow the escape of electrons from the scattering region, the TOF extraction voltage is pulsed for 1.0μs. This sequence is repeated once every 10 μs. The DA signal from vibrationally excited molecules is compared directly to that of the ground-state molecules and the background by first collecting data from vibrationally excited molecules [with pump laser(s) on], then from ground-state molecules (with the pump laser blocked), and then from the background (with the molecular beam blocked) where the signal is collected for each of these three cases for 10 s. These data collection cycles are repeated $50-100$ times per data point.

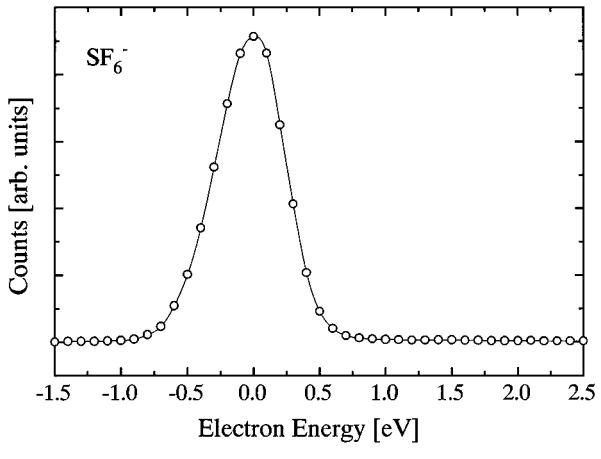

FIG. 3. Electron attachment to SF_6. The SF_6^- rate is measured as a a function of the electron energy. The maximum of the flux distribution is identified as the zero point of the energy.

B. Laser preparation of vibrationally excited sodium dimers

The primary objective of implementing vibrational excitation techniques is to transfer as many molecules as possible from an initial low-lying rovibronic state into a well-defined final distribution of excited states or, ideally, into a single excited quantum state (a review of optical state selection methods can be found in Ref. [53]). The use of a supersonic beam source is essential to attaining this objective. The inherent capacity of such a beam source to cool the internal degrees of freedom provides an ensemble of molecules whose internal state distribution has been compressed into a narrow band of rovibronic states, allowing excitation to take place from a single rovibronic state that contains a relatively large fraction of the entire molecular population. We have choosen the $X^1\Sigma_g^+(v_0''=0,j_0''=9)$ level as our initial pump state, because it resides near the maximum of the population distribution established in our molecular beam. This state contains 8.0% of the total Na_2 population.

As indicated above, we use two distinct methods for preparing vibrationally excited molecules. The technically less demanding method, FCP, is used to perform a general survey of the behavior of the DA rate over a broad range of vibrational levels. The conclusions drawn from the analysis of these data are then tested using the highly selective, but experimentally more demanding, STIRAP technique (see below).

The FCP method of preparing vibrationally excited molecules [53,54] relies on spontaneous emission occurring from a judiciously chosen electronically excited state. Optical fibers guide the output of a single-mode, cw dye laser (Coherent 699-29) to the optical-pumping chamber where

TABLE I. Average vibrational level and average vibrational energy in the Na_2 $X^1\Sigma_g^+$ manifold due to saturated FCP via the $A^1\Sigma_u^+(v',10)\leftarrow X^1\Sigma_g^+(0,9)$ pump transition. The values presented in this table take into account the dependence of the transition dipole moment on internuclear distance.

$(v',10)$	0	1	2	3	4	5	6	7	9	10	13
$\overline{v''}$	5.98	6.8	7.64	8.53	9.48	10.5	11.46	12.42	14.14	14.89	16.96
$\overline{E_{v''}}$(eV)	0.126	0.14	0.155	0.17	0.186	0.203	0.22	0.236	0.264	0.276	0.307

the laser radiation crosses the molecular beam at right angles. The laser is tuned to an $A^1\Sigma_u^+(v',j'=10)\leftarrow X^1\Sigma_g^+(v_0''=0,j_0''=9)$ pump transition, where the exact choice of v', the vibrational quantum number of the intermediate pump state, will dramatically influence the final-state distribution produced by the pumping process. In practice, v' ranges from 0 to 17 in the Na_2 molecule. Once the intermediate $A^1\Sigma_u^+(v',10)$ state is prepared, subsequent spontaneous decay redistributes the original $X^1\Sigma_g^+(0,9)$ population over a range of vibrationally excited v'' levels with $j''=9$ and 11 in the ground electronic state.

The interaction time between the pump laser and the Na_2 molecules is, in our experimental setup, about two orders of magnitude larger than the 12.5-ns lifetime of the Na_2 $A^1\Sigma_u^+$ state, so that each Na_2 molecule can undergo on the order of 100 pump-decay cycles during its passage through the pump laser beam. Excited molecules that decay back to the $X^1\Sigma_g^+(0,9)$ pumped level are excited again until the initial $X^1\Sigma_g^+(0,9)$ level is completely depopulated. The residual population in the $X^1\Sigma_g^+(0,9)$ level is monitored by observing the fluorescence produced by a probe laser downstream from the electron-molecule collision region (see Fig. 2). The probe laser is tuned to the $A^1\Sigma_u^+(17,10)\leftarrow X^1\Sigma_g^+(0,9)$ transition. We accumulate DA data from vibrationally excited Na_2 only when FCP reduces the probe fluorescence to less than 1% of the fluorescence level observed without pumping. The data analysis procedure requires accurate knowledge of the v'' distribution after FCP. This distribution is derived from calculated transition probabilities between the $X^1\Sigma_g^+$ and the $A^1\Sigma_u^+$ states. In the dipole approximation, the transition probability $P(v'',j'';v',j')$ can be expressed as

$$P(v'',j'';v',j')\sim|\langle v'',j''|\mu(R)|v',j'\rangle|^2\nu^3_{v'',j''\leftarrow v',j'}, \quad (1)$$

where the $\nu_{v'',j''\leftarrow v',j'}$ are the transition frequencies. We include the radial dependence of the transition dipole moment $\mu(R)$ [55] in these calculations and arrive at results that differ significantly from the case when $\mu(R)$ is assumed constant [56,57]. The nuclear wave functions $|v,j\rangle$ are obtained by solving the Schrödinger equation using the methods outlined in Ref. [58] in conjunction with the Rydberg-Klein-Rees potentials for the $X^1\Sigma_g^+$ state [59] and the $A^1\Sigma_u^+$ state [60]. A complete listing of the final v'' distribution produced by FCP can be found in Ref. [57]. The vibrational distribution produced by FCP can be characterized by either the level v' excited in the A state, or by the mean vibrational excitation $\overline{v''}_{v'}$ which is given by

$$\overline{v''}_{v'}=\frac{\sum_{v'',j''=9,11} v''\beta(v'',j'')}{\sum_{v'',j''=9,11}\beta(v'',j'')}, \quad (2)$$

where

$$\beta(v'',j'')=|\langle v'',j''|\mu(R)|v',10\rangle|^2\nu^3_{v'',j''\leftarrow v',10}. \quad (3)$$

Table I lists the average vibrational level $\overline{v''}_{v'}$, along with the corresponding average vibrational energies for the vibrational distributions prepared over the course of this experiment.

The primary shortcoming of FCP, namely, its inability to prepare narrow final-state distributions, is addressed by STIRAP, which appears to be an optimal technique for efficient and selective population transfer. STIRAP has grown out of earlier work with Raman lasers [61] and studies of ''self-induced rapid passage'' [62,63]. A detailed description of the physics underlying the STIRAP process and its experimental verification can be found in Refs. [64–66].

In practice, STIRAP requires two laser fields arranged such that molecules encounter the Stokes field, which couples the electronically excited intermediate state v' and the final level v_f'', before the molecules encounter the pump field, which couples the levels $v''=0$ and v'. The Stokes laser is detuned by several power broadened linewidths from an $X^1\Sigma_g^+(v_f'',9)\leftarrow A^1\Sigma_u^+(v',10)$ transition. The pump laser is detuned by an equivalent amount from an $A^1\Sigma_u^+(v',10)\leftarrow X^1\Sigma_g^+(0,9)$ pump transition to maintain two-photon resonances between the laser frequencies and the $v''=0\rightarrow v'\rightarrow v_f''$ transitions. When properly implemented, STIRAP will transfer all of the initial $X^1\Sigma_g^+(0,9)$ population into the *single* vibrationally excited $X^1\Sigma_g^+(v_f'',9)$ target state. We monitor the STIRAP pumping efficiency by tuning the probe laser to an $A^1\Sigma_u^+(v_p'',10)\leftarrow X^1\Sigma_g^+(v_f'',j_f'')$ transition. The resulting fluorescence signal is proportional to the $X^1\Sigma_g^+(v_f'',j_f'')$ population, and the STIRAP pumping efficiency is calibrated by comparing this fluorescence signal to the fluorescence signal produced when the $X^1\Sigma_g^+(v_f'',j_f'')$ state is populated by FCP [65]. The final vibrational levels that are accessible through STIRAP pumping are restricted by the need for relatively large dipole matrix elements and high laser intensities in order to satsify the adiabatic requirement [64–66]. In the present paper, we present DA rates for six individual rovibronic states prepared via STIRAP using the following pumping scheme: $X^1\Sigma_g^+(v_f'',9)\leftarrow A^1\Sigma_u^+(v',10)\leftarrow X^1\Sigma_g^+(0,9)$ with (v_f'',v') chosen to be (10, 5), (12, 5), (14, 6), (22, 9), (23, 9), and (24, 9).

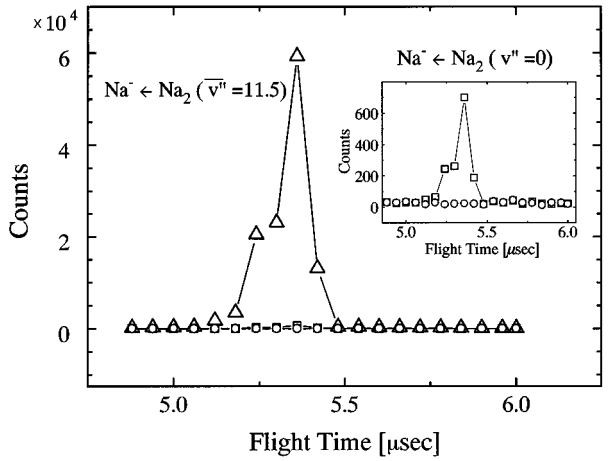

FIG. 4. Time-of-flight spectra for $v''=0$ (□), $\overline{v_6''}=11.5$ (△), and background signal (○). The inset shows the $v''=0$ and the background spectra on an expanded vertical scale.

C. Data accumulation

Figure 4 illustrates several typical TOF spectra: the main panel shows the Na^- signal produced by DA of Na_2 with average vibrational excitation $\overline{v''}=11.5$ (established via FCP through the $v'=6$ intermediate pump level). The signal produced by DA of Na_2 with no vibrational excitation is also shown as is the background signal when the molecular beam is blocked. The mean electron energy was set to approximately 0.4 eV and adjusted to maximize the Na^- signal resulting from $Na_{2(v''=0)}$. The electron energy distribution was kept unchanged for the collection of data from $v''>0$. The inset of Fig. 4 shows the background signal and the Na^- signal produced by Na_2 without vibrational excitation on a magnified scale. The large difference in signal levels that can be achieved through vibrational excitation is obvious.

We calibrate the electron energy by adding from time to time trace amounts of SF_6 as a background gas to the scattering chamber and monitoring the energy dependence of the SF_6^- signal. The predicted threshold energy of the DA process for $Na_{2(v''=0)}$ is approximately 0.2 eV. Therefore, the DA thresholds for vibrational levels $v''>0$ should range between 0.0 and 0.2 eV. Ziesel, Teillet-Billy, and Bouby [17] observed the peak DA cross section of Na_2 in an effusive beam to be 0.05 ± 0.05 eV. At this low electron energy, only molecules in vibrational levels close to the exoergic limit can contribute to the DA signal. In an effusive beam these levels are only weakly thermally populated. The broad distribution of vibrational levels prepared by our laser excitation methods leads us to expect the DA processes anywhere in the range $0.0-0.2$ eV.

III. RESULTS AND ANALYSIS

A. Experimental data and the vibrational dependence of the rate of negative ion formation

The objective is to derive the enhancement of the DA rate

$$\mathscr{E}(v'',j'')=\frac{k(v'',j'')}{k(0,j'')} \tag{4}$$

from the negative ion signals S_L and $S_0(0)$ with and without laser excitation, respectively, where $k(0,j'')$ is the DA rate for the $(v''=0,j'')$ state and $k(v'',j'')$ is the DA rate for the (v'',j'') state. When using the selective STIRAP method to achieve selective vibrational excitation, these signals are related to the rate constants according to

$$S_0(0)=\gamma\sum_{j''}\beta_{\rm th}(0,j'')k(0,j''), \tag{5}$$

where γ is a constant factor relating the rate constants to the signal and $\beta_{\rm th}(0,j'')$ is the relative thermal population of level $(v''=0,j'')$. The value of γ is independent of v'' since the initial kinetic energy of the negative ion (<0.5 eV) is very small compared to the extraction (100 eV) and acceleration (800 eV) energies. Therefore the collection and detection efficiency of the negative ion does not depend on the initial vibrational level of the molecule. In the following argument, we assume that the DA rate is not strongly dependent on j''. If $k(0,j'')=k(0)$, Eq. (5) reduces to

$$S_0(0)=\gamma k(0). \tag{6}$$

The signal produced by laser excitation is

$$S_L(v'')=\gamma[\beta_{\rm th}(0,j'')k(v'')+k(0)-\beta_{\rm th}(0,j'')k(0)]. \tag{7}$$

Combining Eqs. (4)–(6) we find the DA rate produced through STIRAP pumping,

$$\mathscr{E}_{\rm STIRAP}(v'')=\frac{k(v'')}{k(0)}=\frac{1}{\beta_{\rm th}(0,j'')}\frac{S_L(v'')-S_0(0)}{S_0(0)}+1, \tag{8}$$

where j'' refers to the rotational level in the vibrational ground state whose population is transferred to the excited level v''. In this experiment we have used $j''=9$. We have determined experimentally the relative thermal population, $\beta_{\rm th}(0,9)$, to be 0.08. When the Franck-Condon method of vibrational pumping is employed, the DA signal is

$$S_L(v')=\gamma[k(v')+k(0)-\beta_{\rm th}(0,j'')k(0)] \tag{9}$$

with

$$k(v')=\sum_{v''}\beta_{\rm FCP}^{v'}(v'')k(v''), \tag{10}$$

where $\beta_{\rm FCP}^{v'}(v'')$ is the relative population the v'' level established by spontaneous emission from the v' level of the electronically excited state, and $\beta_{\rm FCP}^{v'}(v'')$ is normalized such that

$$\sum_{v''}\beta_{\rm FCP}^{v'}=\beta_{\rm th}(0,9). \tag{11}$$

Instead of Eq. (8) we then have

$$\mathscr{E}_{\rm FCP}(v')=\frac{k(v')}{k(0)}=\frac{1}{\beta_{\rm th}(0,j'')}\frac{S_L(v')-S_0(0)}{S_0(0)}+1. \tag{12}$$

Figure 5 shows $\mathscr{E}_{\rm FCP}(v')$, the enhancement of the DA rate produced by FCP, for a number of vibrational distributions;

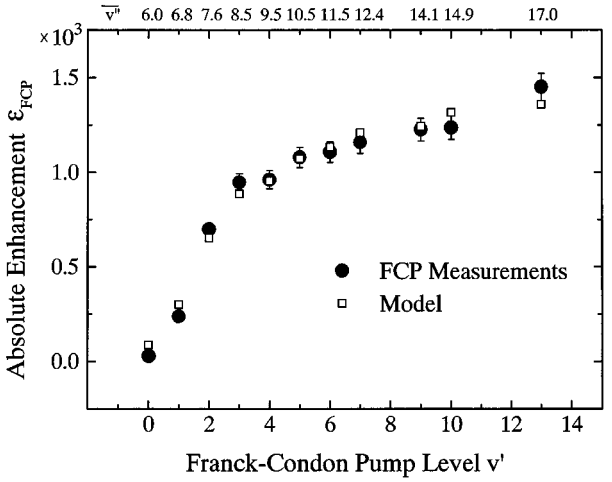

FIG. 5. Measured enhancement of the DA rate (●) as a function of the FCP intermediate pump level v' (lower scale) and the average vibrational state $\overline{v''_{v'}}$ (upper scale). The left-hand scale shows the enhancement of the DA rate with the overall pumping efficiency (8.0%) taken into account. Also shown are the results of our data analysis procedure assuming an exponential dependence of the DA rate constant and $v_c{}' = 12$ (□).

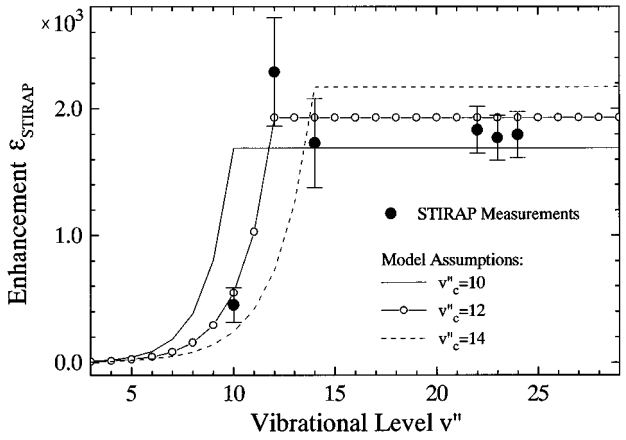

FIG. 6. Measured enhancement of the DA rate (●) for individual rovibronic states prepared through STIRAP pumping. The horizontal scale indicates which $Na_2 X^1\Sigma_g^+(v',9)$ state is prepared and the vertical scale show the enhancement of the DA rate with the overall pumping efficiency (8.0%) taken into account. Also shown are the resulting best fit of our hypothesized vibrational dependence of the DA rate to data generated through FCP assuming an exponential dependence of the DA rate constant (□) and $v''_c = 10$ (solid line), $v''_c = 12$ (solid line with open circles), and $v''_c = 14$ (broken line).

the statistical error (three times the standard deviation) for these data is approximately $\pm 5\%$. The data shown in this figure were previously reported by us in Ref. [47], save the point at $v' = 9$, corresponding to $\overline{v''} = 14.1$, which we have since measured. Furthermore, the average vibrational excitation $\overline{v''}$ associated with each data point differs slightly from that given in Ref. [47] due to improvements made in calculating the $A^1\Sigma_u^+ \leftarrow X^1\Sigma_g^+$ transition probabilities. Figure 5 shows two regions of characteristic behavior for $\mathscr{E}_{FCP}(v')$. In the range $0 < \overline{v''}(v') < 8$, $\mathscr{E}_{FCP}(v')$ increases by about three orders of magnitude, but $\mathscr{E}_{FCP}(v')$ increases by only about 50% more for $\overline{v''}(v') \geqslant 8$. This behavior is reminiscent of that predicted for H_2, D_2, and Li_2 [2–8,10] where the vibrational dependence of the DA cross section changes abruptly when the molecules' internal energy exceeds the potential energy at the crossing of the neutral and negative ion curves. However, because of the relatively low vibrational selectivity of the FCP method, extracting the relative DA rate for individual vibrational levels from FCP data relies on several assumptions as described below.

Guided by the approximate functional form of the theoretically determined DA cross section for H_2, D_2, and Li_2 [2–8] as well as by our experimental results, we assume that the DA rate exhibits the following vibrational dependence:

$$k(v'') = \begin{cases} k_0 e^{\alpha v''} & \text{if } v'' \leqslant v''_c \\ k_{\max} & \text{if } v'' \geqslant v''_c, \end{cases} \tag{13}$$

where k_0 is the DA rate for $v'' = 0$. According to Eq. (13) the DA rate increases exponentially until it reaches its saturation value of $k_{\max} = k_0 e^{\alpha v''_c}$ at the critical vibrational level v''_c. Above v''_c, the DA rate remains constant. As defined here, v''_c is reminiscent of the exoergic threshold that theoretical studies [2–8] predict should delineate the region where the DA rate increases approximately exponentially with v'' from the region where the DA rate is only weakly dependent on v''. The enhancement of the DA rate can now be determined by combining Eqs. (10) and (13), yielding $\mathscr{E}_{FCP}(v') = k(v')/k(0)$. When any two of the three parameters $k_{\max}/k_0$, α, and v''_c are chosen the third one is fixed as well. In Eq. (12), v'_c and the maximum enhancement of the DA rate, $k_{\max}/k_0$, serve as free parameters. For various choices of v''_c; the value of $k_{\max}/k_0$ is derived from a least-squares fit of Eq. (12) to the experimentally determined $\mathscr{E}_{FCP}(v')$. The results are shown in Fig. 5. Due to the relatively broad vibrational distributions, this fit is not very sensitive to the value of v''_c; nevertheless, we are able to confine v''_c to the range $10 \leqslant v''_c \leqslant 14$.

The highly selective STIRAP method remedies the shortcoming of the FCP method by yielding state specific enhancements of the DA rate, $\mathscr{E}_{STIRAP}(v'')$, without the need for further model-dependent data analysis. Figure 6 shows the enhancement of the DA rate produced by STIRAP pumping along with the least-squares fit of Eq. (12) to FCP data when v''_c is taken to be 10, 12, and 14. The enhancement $\mathscr{E}_{STIRAP}(v'')$ determined from the experiment at very high vibrational excitation is compatible with our model for $10 \leqslant v''_c \leqslant 12$, while the enhancement for small v'' is compatible with $12 \leqslant v''_c \leqslant 14$. Two observations are evident from these data. First, the enhancement of the DA rate for rovibronic levels well above the exoergic limit, i.e., for the (v'',j'') levels (22, 9), (23, 9), and (24, 9), is independent of v'' within the limits of the experimental uncertainty. Second, the behavior of the DA rate from low to high v'' clearly points to $v'' = 12$ as the critical level v''_c, i.e., the level that marks a significant change in the vibrational dependence of the DA rate. These results also fix the value of $k_{\max}/k_0$ at 1.9×10^3. The STIRAP data point at $v'' = 12$ suggests a larger DA rate as compared to $v'' > 12$; however, further experiments will be required to reduce the error bars before a

TABLE II. Characteristic data for the Na_2 and Na_2^- potential curves.

		Calc.	Expt.	Other calc.
Na	EA (eV)	0.547	0.548 [68]	0.541 [24]
Na_2	D_e (eV)	0.744	0.746 [67]	0.679 [24]
	R_e (nm)	0.3073	0.3079 [67]	0.3189 [24]
	ω_e (cm^{-1})	158.335	159.100 [67]	149.500 [24]
	EA (eV)	0.437		0.463 [24]
Na_2^-	D_e (eV)	0.638		0.569 [24]
	R_e (nm)	0.3494		0.3650 [24]
	ω_e (cm^{-1})	103.153		98.500 [24]
Na_2/Na_2^-	$E(R_s)$ (eV)	0.229		0.204 [22]
	R_s (nm)	0.3958		0.4101 [22]
Na_2	$E_{vib}(v''=11)-E(R_s)$ (cm^{-1})	-118.2		
	$E_{vib}(v''=12)-E(R_s)$ (cm^{-1})	22.6		

conclusive statement can, based on experimental data, be made.

The accuracy of the absolute value for k_{max}/k_0 depends on the accuracy to which the absolute transfer efficiency is known. Since the $X^1\Sigma_g^+(22,9)$ level was prepared through STIRAP pumping with a transfer efficiency $T=0.98$ (as measured by laser-induced fluorescence techniques) we expect no more than a 2% uncertainty in the resulting value of k_{max}/k_0. The $X^1\Sigma_g^+(23,9)$ level and the $X^1\Sigma_g^+(24,9)$ level were prepared with $T\geqslant 0.90$. The question therefore arises as to the fate of the missing fraction of molecules orginally in the $X^1\Sigma_g^+(0,9)$ level. Do these molecules remain in the initial $X^1\Sigma_g^+(0,9)$ level, or are they dispersed over a distribution of vibrationally excited levels? By using two probe lasers to simultaneously monitor the population in the initial and the final levels, we confirmed that $\geqslant 95\%$ of the population initially in the $X^1\Sigma_g^+(0,9)$ state either remains in the initial state or is transferred to the final $X^1\Sigma_g^+(v_f'',9)$ state. Consequently, the uncertainty of the maximun enhancement k_{max}/k_0 due to the uncertainty in the absolute value of T is less than 5%.

B. Theoretical characterization of the resonance state $A^2\Sigma_g^+$

In order to provide the basis for a theoretical analysis of the vibrational enhancement of DA in collisions of low-energy electrons with Na_2, we have performed electronic structure calculations based on pseudopotential valence-electron multireference configuration interactions (MR-CI) as well as all-electron self-consistent field (SCF) valence MR-CI with an effective core polarization potential as described in Refs. [69,70]. Both approaches have been shown to yield dissociation energies, excitation energies, and electron affinities of alkali dimers to better than 100 cm^{-1} [69–71], provided reasonably saturated basis sets are used. Figure 1 displays bound state potential curves for Na_2 $X^1\Sigma_g^+$ and Na_2^- $X^2\Sigma_u^+$, $A^2\Sigma_g^+$ as obtained with an $8s$, $6p$, $3d$ valence shell Gaussian-type orbital (GTO) basis for each Na and a $3s$, $3p$ GTO set at the center of the molecule. Some pertinent atomic data and characteristic data of these potentials are collected in Table II. Comparison with experimental data and other theoretical results serves to establish the reliability of our results.

For internuclear distances $R>0.4$ nm, the bound A state shows a remarkably flat shape in spite of the dominance of the core-excited (or Feshbach) configuration $1\sigma_g 1\sigma_u^2$ (core orbitals are not counted). This may be understood from the fact that strong s-p mixing enhances the bonding effect of the $1\sigma_g$ orbital but reduces the antibonding effect of the $1\sigma_u$ orbital. In addition, for decreasing internuclear seperations R, this state aquires an increasing contribution from the shape-type structure $1\sigma_g^2 2\sigma_g$, which actually amounts to 30% at $R=0.4$ nm. The inset in Fig. 1 displays the crossing region in more detail and also indicates the vibrational energy levels of Na_2 (X). The decrease of the A-state potential prior to its crossing with Na_2 (X) is a real effect and is connected with the electron distribution becoming rapidly more diffuse as the crossing point is approached. The continuation below the crossing (lower dashed curve) gives the energies as obtained variationally from the finite basis used and is therefore an artifact depending mainly on the exponent of the most diffuse s function (0.003 in our case). The proper definition of the resonance state is rather involved and, rigorously, requires full-scale electron scattering calculations for $Na_{2(R)+e^-(\epsilon)}$, which are not attemped here. A simple Feshbach projection based on removing all shape-type configurations $1\sigma_g^2 n\sigma_g$ produces a pure Feshbach state (upper dashed line in Fig. 1) which is subject to a large shift due to its strong interaction with the continuum. Thus, on the one hand, the resonance state requires at least one shape configuration $1\sigma_g^2 2\sigma_g$. On the other hand, the free variation of its 2 σ_g orbital would turn this into a very diffuse representation of an unbound electron of low energy, and the shape configuration would then dominate the state leading to the lowest dashed line in Fig. 1. Therefore the variation of the $2\sigma_g$ has to be constrained. Instead of restricting the range of the $2\sigma_g$ orbital by arbitrarily limiting the basis set, we use the following approach: All shape configurations $1\sigma_g^2 n\sigma_g$ for $n>2$ are removed from the configuration space and the orbital optimization in the multiconfiguration-SCF step is constrained by prescribing a fixed ratio for the coefficients of the two leading configurations $1\sigma_g^2 2\sigma_g$ and $1\sigma_g 1\sigma_u^2$. This preserves a relatively compact shape of the $2\sigma_g$ orbital reflecting optimal interaction between the two configurations. Such a constraint is, of course, lifted in the following MR-CI step. The ratio has been chosen as 0.5, which is close to its value

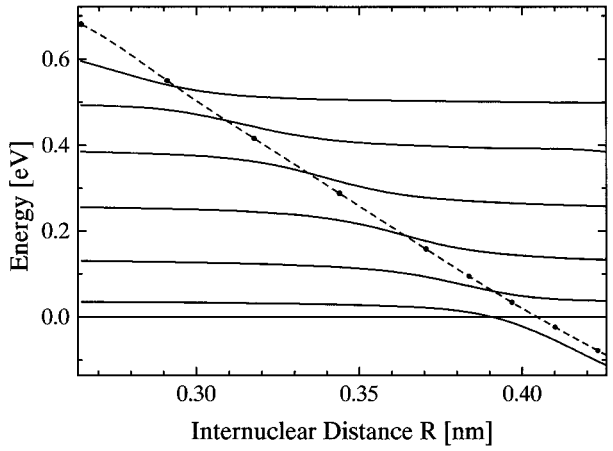

FIG. 7. Excess electron energies calculated as $E[\mathrm{Na_2}^-(^2\Sigma_g^+)]-E[\mathrm{Na_2}(X^1\Sigma_g^+)]$ from MR-CI using very diffuse basis functions and an electron-confining potential (see text). Dashed line: resonance state as in Fig. 1.

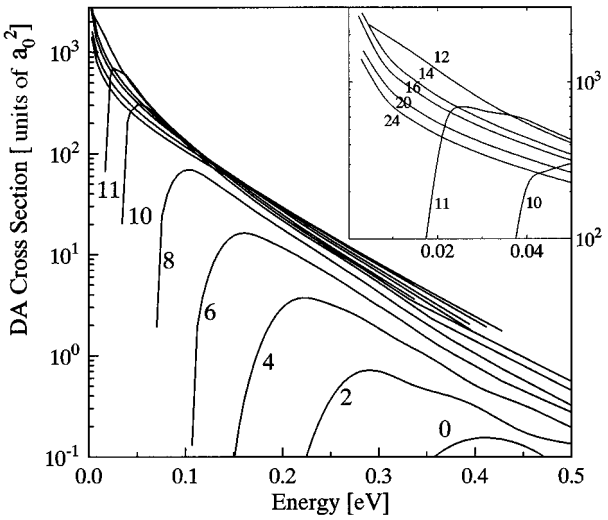

FIG. 8. Calculated dissociative attachment cross sections (in a_0^2) as a function of incident electron energy for rovibrational states of Na_2 with $j''=9$ and v'' ranging from 0 to 24.

for the A state at $R=0.42$ nm. This procedure results in the potential represented as the middle dashed line in Fig. 1. Reassuringly, the potential is rather stable against changes of the constraining ratio.

Further support for this potential may be drawn from Fig. 7, which displays preliminary results for excess electron energies [defined as energy differences between $\mathrm{Na_2}^-(A^2\Sigma_g^+)$ states and the $\mathrm{Na_2}(X^1\Sigma_g^+)$ state] as obtained from MR-CI calculations where the molecule has been placed in an electron-confining potential with a range of about 3 nm. The resonance potential is seen to match well with the visible perturbations of the discretized continuum. The resonance-state potential crosses the $X^1\Sigma_g^+$ potential at $R=0.396$ nm and at an energy of 0.229 eV with respect to the $X^1\Sigma_g^+$ equilibrium energy. This places the crossing very close to the classical outer turning of the $v''=12$ vibrational level, in gratifying agreement with the conclusions from the measurements. (Note that the exoergic limit lies between the levels $v''=10$ and $v''=11$.) At shorter distances our resonance state potential is considerably more repulsive than that suggested in Ref. [22]. The vertical attachment energy is about ~ 0.4 eV, i.e., ~ 0.2 eV above the crossing energy. For the corresponding state of $\mathrm{Li_2}^-$, a pronounced minimum with a vertical attachment energy of ~ 0.3 eV was reported [23]. It remains to be seen whether these differences in the shape of the potentials or differences in the width functions are mainly responsible for the quite different vibrational enhancements calculated for Li_2. Further work is in progress to extract, from the calculations whose results are displayed in Fig. 7, electron phase shifts and the resonance width required for a detailed analysis of the detachment dynamics.

C. Theoretical enhancement factors

Even though a full description of the electron attachment process in terms of electron phase shifts or width and shift functions is not yet available, we may derive theoretical enhancement factors using the traditional resonance theory in an approximation similar to that previously applied to, e.g., H_2 [2,5] and Li_2 [3]. The resonance-continuum coupling is simply related to the electron energy by Wigner's threshold law for s partial waves, i.e., $V_c(\epsilon)=V_0\epsilon^{1/4}$. The local resonance width is derived from the difference potential via the resonance conditions $\epsilon_r(R)=V_{A^-}(R)-V_X(R)$ as $\Gamma(R)=2\pi V_c^2[\epsilon_r(R)]$. The cross section for dissociative attachment of an electron with energy ϵ to Na_2 in its rovibrational state $\chi^0_{v''j''}$ is obtained as

$$\sigma_{\mathrm{DA}}(v'',\epsilon)=\frac{\pi^2}{\epsilon}\frac{\hbar k}{M}\lim_{R\to\infty}|\chi_{v''j''}(R)|^2, \tag{14}$$

where M is the reduced mass of Na_2 and k the assymptotic wave vector of the separating nuclei. $\chi_{v''j''}(R)$ is the solution of

$$\left(T_N+V_A^-(R)-\frac{i}{2}\Gamma(R)-E_{v''j''}-\epsilon\right)\chi_{v''j''}(R) = -V_c(\epsilon)\chi^0_{v''j''}(R) \tag{15}$$

with the outgoing wave boundary condition, $\chi(R)\to\exp[i(kR+\delta)]$. The coupling strength V_0 has been adjusted to the observed enhancements—best agreement was found for $\Gamma_0=2\pi V_0^2=0.026$ a.u. Furthermore, the calculated resonance potential has been slightly shifted to match the calculated crossing point accurately. The theoretical cross sections are shown in Fig. 8. For vibrational levels $v''\geqslant 12$, the low-energy cross sections behave as $\epsilon^{-1/2}$ due to the assumption made for $V_c(\epsilon)$. The strong DA enhancements are then largely due to the contributions of slow electrons, $\epsilon\leqslant 20$ meV. As in the experiment, the electron flux distribution obtained in the SF_6 electron attachment measurement (Fig. 3) has been shifted in energy to maximize the $v''=0$ DA rate, resulting in a peak energy of 0.4 eV. The enhancement factors obtained from this flux distribution are shown in Fig. 9 as solid line. There is quite reasonable agreement with the STIRAP measurements, apart from the distinctive slope in the theoretical enhancement factors for $v''\geqslant 14$. In view of the uncertainty in the threshold electron flux distribution we

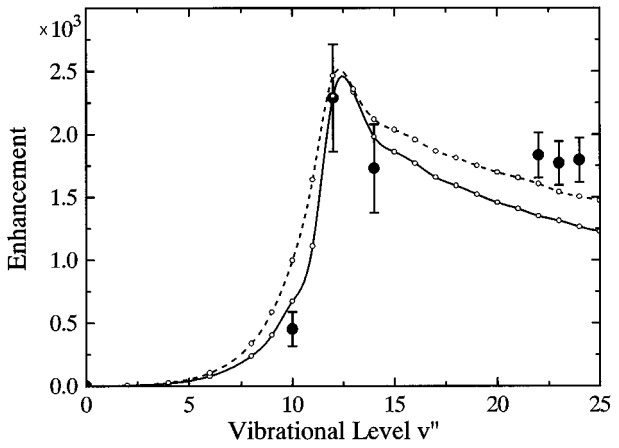

FIG. 9. Theoretical enhancement factors of the DA rate. Solid line: electron flux distribution as shown in Fig. 3 with peak at 0.4 eV; $\Gamma_0 = 0.026$ a.u., dashed line: flux distribution damped for low ϵ, see text; $\Gamma_0 = 0.0275$ a.u., and solid circle: experimental values from the STIRAP measurements.

show for comparison enhancement factors obtained from a distribution damped by $1-\exp(-\epsilon/12meV)$ and a corresponding change of Γ_0 to 0.0275 a.u. The slope at high v'' appears to be reduced but a larger discrepancy is observed for $v''=10$. The significant contribution from near threshold electrons underlines that a more conclusive comparison between theory and expriment requires, in addition to the full specification of $V_c(R,\epsilon)$ and a better energy resolution of the electron beam, a thorough analysis of nonlocal effects in the attachment process.

IV. CONCLUSION

Using Franck-Condon pumping to prepare vibrationally excited Na_2, we observe a dramatic increase in the DA rate as a function of vibrational excitation at low $\overline{v''}$, followed by a much lower sensitivity of the DA rate to vibrational excitation at high $\overline{v''}$. The data generated with FCP are modeled accurately by assuming a vibrational dependence of the dissociative attachment rate according to Eq. (13), which determines the critical vibrational level as $v_c''=12\pm2$. The maximum enhancement occurs when $v''>v_c''$ and is $k_{\max}/k_0=1.9\pm0.1\times10^3$. The error is primarily due to the uncertainty inherent in determining the relative population of the initial $X^1\Sigma_g^+(0,9)$ level [see Eq. (12)]. Using the method of stimulated Raman scattering with adiabatic passage to prepare individual rovibronic states, the observed behavior of the DA rate substantiates the validity of the model defined in Eq. (13). STIRAP based data furnish a maximum enhancement $k_{\max}/k_0$ of 1.9×10^3 and suggest that $v_c=12$. These results compare well with our *ab initio* calculations, which predict a crossing between the neutral and ionic potential energy curves at an internuclear distance close to the outer turning point of the vibrational level $v''=12$.

Future work is planned to study the vibrational dependence of the DA rate in more detail. An electron source with energy resolution of the order of a few meV and a current of about 0.5 nA, created by two-step photoionization (using a cw dye laser and a frequency doubled mode locked titanium:sapphire laser) of the ubiquitous atomic sodium present in the Na_2 beam [72], will provide accurate control over the incident electrons' kinetic energy and will complement the precise internal state control achieved in the present study.

ACKNOWLEDGMENTS

This work has been supported by the Deutsche Forschungsgemeinschaft, the EU network ''Laser controlled dynamics of molecular processes and applications'' (ERB-CHR-XCT-94-0603), and the ''Stiftung für Innovation Rheinland Pfalz'' through the ''Laserzentrum Kaiserslautern.'' The work of one author (A. K.) was supported in part by the German Academic Exchange Service (DAAD).

[1] M. Allan and S. F. Wong, Phys. Rev. Lett. **41**, 1791 (1978).
[2] J. M. Wadehra and J. N. Bardsley, Phys. Rev. Lett. **41**, 1795 (1978).
[3] J. M. Wadehra, Phys. Rev. A **41**, 3607 (1990).
[4] J. M. Wadehra, Appl. Phys. Lett. **35**, 917 (1979); Phys. Rev. A **29**, 106 (1984).
[5] J. N. Bardsley and J. M. Wadehra, Phys. Rev. A **20**, 1398 (1979).
[6] J. P. Gauyacq, J. Phys. B **18**, 1859 (1985).
[7] C. Mündel, M. Berman, and W. Domcke, Phys. Rev. A **32**, 181 (1985).
[8] A. P. Hickman, Phys. Rev. A **43**, 3495 (1991).
[9] D. Teillet-Billy and J. P. Gauyacq, J. Phys. B **17**, 4041 (1984).
[10] W. Domcke, Phys. Rep. **208**, 97 (1991).
[11] W. L. Fite and R. T. Brackmann, in *Proceedings of the Fourth International Conference on the Physics of Electronic and Atomic Collisions* (Science Bookcrafters Inc., Hastings-on-Hudson, New York, 1965), p. 100.
[12] W. R. Henderson, W. L. Fite, and R. T. Brackmann, Phys. Rev. **183**, 157 (1969).
[13] D. Spence and G. J. Schulz, Phys. Rev. **188**, 280 (1969).
[14] J. N. Bardsley, A. Herzenberg, and F. Mandl, Proc. Phys. Soc. London **89**, 305 (1966); **89**, 321 (1966).
[15] D. Popovic, I. Čadež, M. Landau, C. Schermann, and R. I. Hall, Meas. Sci. Tech. **1**, 1040 (1990).
[16] D. Rapp and D. D. Briglia, J. Chem. Phys. **43**, 1481 (1965).
[17] J. P. Ziesel, D. Teillet-Billy, and L. Bouby, Chem. Phys. Lett. **123**, 371 (1986).
[18] T. F. O'Malley, Phys. Rev. **155**, 59 (1967).
[19] T. F. O'Malley, Phys. Rev. **150**, 14 (1966).
[20] J. M. Wadehra, in *Nonequilibrium Vibrational Kinetics*, edited by M. Capitelli (Springer-Verlag, Heidelberg 1986), p. 191.
[21] D. D. Konowalow and J. L. Fish, Chem. Phys. Lett. **104**, 210 (1984).
[22] K. K. Sunil and K. D. Jordan, Chem. Phys. Lett. **104**, 343 (1984).

[23] H. H. Michels, R. H. Hobbs, and L. A. Wright, Chem. Phys. Lett. **118**, 67 (1985).
[24] H. Partridge, D. A. Dixon, S. P. Walch. C. W. Bauschlicher Jr., and J. L. Gole, J. Chem. Phys. **79**, 1859 (1983).
[25] M. W. McGeoch and R. E. Schlier, Phys. Rev. A **33**, 1708 (1986).
[26] D. Spence and G. J. Schulz, J. Chem. Phys. **54**, 5424 (1971).
[27] F. K. Truby, Phys. Rev. **188**, 508 (1969).
[28] H. L. Brooks, S. R. Hunter, and K. J. Nygaard, J. Chem. Phys. **71**, 1870 (1979).
[29] M. Allan and S. F. Wong, J. Chem. Phys. **74**, 1687 (1981).
[30] P. J. Chantry, J. Chem. Phys. **51**, 3369 (1969).
[31] F. C. Fehsenfeld, J. Chem. Phys. **53**, 2000 (1970).
[32] B. Lehmann, Z. Naturforsch. **25**, 1755 (1970).
[33] D. Spence and F. J. Schulz, J. Chem. Phys. **58**, 1800 (1973).
[34] L. E. Kline, D. K. Davies, C. L. Chen, and P. J. Chantry, J. Appl. Phys. **50**, 6789 (1979).
[35] M. Fenzlaff, R. Gerhard, and E. Illenberger, J. Chem. Phys. **88**, 149 (1988).
[36] P. G. Datskos and L. G. Christophorou, J. Chem. Phys. **90**, 2626 (1989).
[37] P. G. Datskos, L. G. Christophorou, and J. G. Carter, Chem. Phys. Lett. **168**, 324 (1990).
[38] P. G. Datskos, L. G. Christophorou, and J. G. Carter, J. Chem. Phys. **97**, 9031 (1992).
[39] W. E. Wentworth, R. George, and H. Keith, J. Chem. Phys. **51**, 1791 (1960).
[40] S. M. Spyrou and L. G. Christophorou, J. Chem. Phys. **82**, 2620 (1985).
[41] S. M. Spyrou and L. G. Christophorou, J. Chem. Phys. **83**, 2829 (1985).
[42] P. G. Datskos and L. G. Christophorou, J. Chem. Phys. **86**, 1982 (1987).
[43] I. Čadež, R. I. Hall, M. Landau, F. Pichou, and C. Schermann, J. Phys. B **21**, 3271 (1988).
[44] S. K. Srivastava and O. J. Orient, Phys. Rev. A **27**, 1209 (1983).
[45] C. L. Chen and P. J. Chantry, J. Chem. Phys. **71**, 3897 (1979).
[46] I. M. Beterov and N. V. Fateyev, Opt. Commun. **40**, 425 (1982).
[47] M. Külz, A. Kortyna, M. Keil, B. Schellhaaß, and K. Bergmann, Phys. Rev. A **48**, R4015 (1993).
[48] K. Bergmann, U. Hefter, and P. Hering, Chem. Phys. **32**, 329 (1978).
[49] K. Bergmann, W. Demtröder, and P. Hering, Appl. Phys. **8**, 65 (1975).
[50] R. E. Collins, B. B. Aubrey, P. N. Eisner, and R. J. Celotta, Rev. Sci. Instrum. **41**, 1403 (1970).
[51] W. C. Wiley and I. H. McLaren, Rev. Sci. Instrum. **26**, 1150 (1955).
[52] D. Klar, M. W. Ruf, and H. Hotop, Aust. J. Phys. **45**, 263 (1992).
[53] K. Bergmann, in *Atomic and Molecular Beam Methods* edited by G. Scoles (Oxford University Press, New York 1988), p. 293.
[54] K. Bergmann, U. Hefter, and J. Witt, J. Chem. Phys. **72**, 4777 (1980).
[55] I. Schmidt, Dissertation, Fachbereich Chemie der Universität Kaiserslautern, 1987, p. 133.
[56] M. Külz, A. Kortyna, M. Keil, B. Schellhaaß, and K. Bergmann, Z. Phys. D **33**, 109 (1995).
[57] B. Schellhaaß, Diplomarbeit, Fachbereich Physik der Universität Kaiserslautern, 1994, p. 100.
[58] H. J. Korsch and H. Laurent, J. Phys. B **14**, 4213 (1981); J. Stoer, *Numerische Mathematik*, 3rd ed. (Springer-Verlag, Berlin, 1980), Vol. 2.
[59] P. Kusch and M. M. Hessel, J. Chem. Phys. **68**, 2591 (1978).
[60] G. Gerber and R. Möller, Chem. Phys. Lett. **113**, 546 (1985).
[61] M. Becker, U. Gaubatz, and K. Bergmann, J. Chem. Phys. **87**, 5064 (1978).
[62] D. Grischkoksky, M. M. T. Loy, and P. F. Liao, Phys. Rev. A **12**, 2514 (1975).
[63] M. M. T. Loy, Phys. Rev. Lett. **36**, 1454 (1976).
[64] J. R. Kuklinski, U. Gaubatz, F. T. Hioe, and K. Bergmann, Phys. Rev. A **40**, 6741 (1989).
[65] U. Gaubatz, P. Rudecki, S. Schiemann, and K. Bergmann, J. Chem. Phys. **92**, 5363 (1990); G.- H. He, A. Kuhn, S. Schiemann, and K. Bergmann, J. Opt. Soc. Am. B **7**, 1960 (1990).
[66] K. Bergmann and B. W. Shore, in *Molecular Dynamics and Spectroscopy by Stimulated Emission Pumping*, Advances in Physical Chemistry, edited by H. C. Dai and R. W. Field (World Scientific, Singapore, 1995).
[67] H. Hotop and W. C. Lineberger, J. Phys. Chem. Rev. Data **4**, 539 (1975).
[68] H. Hotop and W. C. Lineberger, J. Phys. Chem. Rev. Data **14**, 731 (1985); Ref. Data **4**, 73 (1985).
[69] W. Müller, J. Flesch, and W. Meyer, J. Chem. Phys. **80**, 3297 (1984); W. Müller and W. Meyer, *ibid.* **80**, 3311 (1984); N. Spies, Dissertation, Fachbereich Chemie der Universität Kaiserslautern.
[70] H. J. Werner and E. A. Reinsch, J. Chem. Phys. **76**, 3144 (1982).
[71] I. Schmidt-Mink, W. Müller, and W. Meyer, Chem. Phys. Lett. **112**, 120 (1984); I. Schmidt-Mink and W. Meyer, *ibid.* **121**, 49(1985).
[72] J. Hauck, Diplomarbeit, Fachbereich Physik der Universität Kaiserslautern, 1995.